jove

Vapor Phase Deposition of Electroactive Poly(3,4-ethylenedioxythiophene) onto Electrospun Commodity Polymer Nanofibers

Shuvo Brahma[1], **Aidan Gustafson**[2,3], **Junaid ur Rehman**[1], **Nicholas R. Lontkowski**[2], **Alyssa Libonati**[3], **Marcus Goss**[4], **R. Kōnane Bay**[3], **Jennifer A. Irvin**[1,2,5], **Tania Betancourt**[1,2]

[1] Material Science, Engineering and Commercialization, Texas State University [2] Department of Chemistry and Biochemistry, Texas State University [3] Chemical and Biological Engineering, University of Colorado Boulder [4] STAR Park, Texas State University [5] College of Science and Engineering, University of Houston-Clear Lake

Corresponding Authors

Jennifer A. Irvin
irvinj@uhcl.edu

Tania Betancourt
tania.betancourt@txstate.edu

Citation

Brahma, S., Gustafson, A., ur Rehman, J., Lontkowski, N.R., Libonati, A., Goss, M., Bay, R.K., Irvin, J.A., Betancourt, T. Vapor Phase Deposition of Electroactive Poly(3,4-ethylenedioxythiophene) onto Electrospun Commodity Polymer Nanofibers. *J. Vis. Exp.* (217), e67825, doi:10.3791/67825 (2025).

Date Published

March 7, 2025

DOI

10.3791/67825

URL

jove.com/video/67825

Abstract

This study investigates the preparation of polyacrylonitrile (PAN) nanofibers through electrospinning to create highly porous and strong materials for applications in water purification, electrocatalysis, and biomedicine. The uniformly white PAN nanofiber mats were cut into 2 cm x 2 cm coupons to ensure consistency. After electrospinning, these nanofibers were coated with an electroactive polymer (EAP) using chemical vapor deposition, with iron (III) chloride ($FeCl_3$) serving as an oxidant for polymerizing 3,4-ethylenedioxythiophene (EDOT) into poly(3,4-ethylenedioxythiophene) (PEDOT). The study examined the impact of different $FeCl_3$ concentrations on PEDOT deposition on the PAN coupons. PEDOT deposition led to an increase in coupon weight. Scanning electron microscopy (SEM) revealed increases in the diameter of the nanofibers treated with increasing $FeCl_3$ oxidant concentration, although higher $FeCl_3$ concentrations caused inter-fiber bridging, implying a concomitant decrease in inter-fiber spacing. Energy dispersive X-ray spectroscopy (EDS) was used to confirm the presence of Fe, Cl, and S in the nanofibers, with sulfur content rising with $FeCl_3$ concentration used, suggesting increased PEDOT deposition efficiency with increasing oxidant concentration. Mechanical testing showed that PEDOT-coated PAN fibers had improved tensile strength and toughness in the hydrated state compared to pure PAN nanofibers. These results highlight the crucial role of $FeCl_3$ concentration in influencing the morphology and properties of PAN-PEDOT composites, enhancing their suitability for applications such as water purification, tissue engineering, biosensing, catalysis, and energy storage.

Introduction

Electrospinning is a technique utilized for the fabrication of nanofiber-based materials for applications including tissue engineering, drug delivery, biosensing, food encapsulation, insulating materials, energy storage and dissipation, catalysis, and filtration. The versatility of this technique allows for different fiber arrangements and morphological structures, supporting innovations in multiple industries[1,2,3,4,5,6]. Electrospinning is a voltage-driven fabrication technique that produces small fibers from a polymer solution. The basic setup includes a syringe fitted with a spinneret (a stainless-steel needle or capillary extrusion tube) that is filled with a polymer solution, a syringe pump, a high-voltage power source, and a collector, as shown in **Figure 1A**. The syringe pump ensures a constant flow of the polymer solution. Using a rotating drum as a collector allows for the preparation of larger, more uniform fiber mats; rotation at low speeds yields randomly oriented fibers, while rotation at high speeds yields fibers oriented in the direction of drum rotation[3]. The speed necessary for fiber alignment is polymer solution-specific and can vary depending on factors such as solution viscosity, surface tension, and concentration. The process begins when an electric field is established between the needle tip and the collector, resulting in charges accumulating on the liquid surface. When electrostatic repulsion overcomes the surface tension, the liquid polymer solution forms a Taylor cone, leading to a jet of charged liquid moving toward the collector. As the solvent evaporates, solid polymer fibers are deposited onto the collector[4,5]. Electrospun nanofibers have been made from several polymers including polyacrylonitrile (PAN), polystyrene (PS), poly(vinyl alcohol) (PVA), polycaprolactone (PCL), poly(ethylene oxide) (PEO), poly(lactic-co-glycolic acid) (PLGA), nylon, poly(vinylidene fluoride)/polyurethane and polyvinylpyrrolidone[1,7,8,9,10,11,12].

The fabrication of electrospun nanofiber-based materials using electroactive polymers (EAPs) is of particular interest. EAPs are materials with conjugated backbones that can be reversibly switched between multiple oxidation states using either chemical or electrochemical processes. This modification leads to changes in properties such as color, conductivity, reactivity, and volume[13]. This versatility makes EAPs well-suited for applications such as energy conversion and storage, electrochromics, actuators, sensors, and bioelectronics devices. EAP nanofibers, more specifically, have potential applications in energy storage, sensors, actuators, separations, nerve/tissue engineering, and biosensing[14]. Electroactive polymers (EAPs) pose several challenges during electrospinning due to their low viscosity and high conductivity which can hinder stable jet formation and lead to jet instability and bead formation instead of continuous fibers. Their sensitivity to electric fields can cause premature deformation or activation, resulting in inconsistent fiber formation. Additionally, EAPs typically suffer from poor solubility, requiring the use of specifically suitable solvents that affect solution viscosity, surface tension, and dielectric properties, complicating the process. The mechanical properties of EAPs, such as low elasticity and flexibility, can lead to jet breakage and fiber inconsistency. At the same time, the electrospinning process parameters, including voltage, needle-collector distance, and flow rate, need careful optimization, making the process more complex and less reproducible[15,16,17,18]. While there are several notable exceptions, in most cases, it is not possible to electrospin solutions of EAPs without the incorporation of

additional polymers, called carrier polymers, that are capable of electrospinning[19].

Alternative methods have been devised for the preparation of EAP nanofiber-based materials. Blending EAPs with other polymers or nanoparticles yields properties that are a hybrid of the two polymers[1]. While blending EAPs with carrier polymers enables electrospinning, the desirable properties of the EAP — notably its electroactivity (ability to change its properties in the presence of an electric field) and its conductivity — may be lost when blended. Instead, coating nonelectroactive electrospun nanofibers with EAPs can be a way to provide the electroactivity and conductivity of the EAP at the surface while having a mechanically robust polymer at the core of the nanofibers. EAP coatings can be accomplished using electrodeposition, spray coating, dip coating, or vapor-phase deposition. However, electrodeposition has several drawbacks. It requires conductive substrates, limiting its use with non-conductive materials unless they undergo pre-treatment to enhance conductivity. Achieving uniform coatings on complex or porous surfaces can be challenging due to uneven electric fields, resulting in variable deposition thicknesses. Controlling the morphology, thickness, and crystallinity of the coating also requires precise tuning of the electrolyte composition and applied voltage. Additionally, large-scale or three-dimensional objects may not receive uniform coatings, particularly in recessed areas. The risk of contamination from impurities in the electrolyte or on the electrode surface can introduce defects, while energy-intensive processes further complicate the technique[19]. Dip coating is a process where substrates are immersed in an EAP polymer solution and then withdrawn at a controlled rate to create a thin film. Alternatively, dip coating of a substrate with a monomer solution could be followed by a secondary polymerization step. The choice of solvent is critical; it must dissolve the polymer or monomer without dissolving the underlying fibers. However, the formation of non-conformal coatings or aggregation can be a drawback, particularly on complex surfaces. Spray coating efficiently covers large or complex surfaces and can be combined with other methods for multi-layer applications[20], but spray coating also requires careful solvent selection to avoid dissolving the substrate polymers. Vapor phase deposition, specifically chemical vapor deposition (CVD), typically avoids solubility issues, produces uniform, thin coatings with excellent adhesion, allows coverage of complex geometries, and is a scalable process. CVD is a widely used method for uniformly coating substrates with various materials, such as carbon, metal oxides, and EAPs, by vaporizing precursors, transporting them to the substrate, and enabling adsorption, nucleation, and growth under controlled conditions. In the case of CVD of EAPs, the process typically involves vaporizing monomers and/or oxidants to enable *in situ* oxidative polymerization to take place onto the fibers. CVD offers advantages like uniform and conformal coatings, precise thin film formation, scalability for industrial applications, and versatility in material deposition, enhancing the functionality of nanofibers for diverse applications[21]. CVD was used by Zhu et al. for the coating of calcinated $NiCo_2O_4$ nanofibers originally made with polyvinylpyrrolidone with the EAP polypyrrole[22].

In our work, nanofiber mats have been prepared from PAN as substrates for the CVD of EAPs. PAN is an inexpensive commodity polymer that is insoluble in aqueous media, is environmentally stable, and has high strength and modulus. Recent study by Sapountzi et al.[23] has demonstrated the successful deposition of various materials on PAN nanofibers using CVD techniques. Specifically, they electrospun solutions of PAN containing the oxidant ferric chloride and then exposed the fibers to pyrrole and/

or pyrrole-3-carboxylic acid vapors to produce core-shell nanofibers of PAN and EAPs for glucose sensing[23].

In the CVD of EAPs, the concentration of oxidant is crucial to enable the oxidative polymerization of electroactive monomers like pyrrole and aniline onto electrospun nanofibers, significantly influencing the deposition rate and properties of the resulting conducting polymers. Ferric chloride ($FeCl_3$) is commonly used as an oxidizing agent, forming monomer radical cations that react to create polymers[24,25]. Higher $FeCl_3$ concentrations increase the polymerization and deposition rates due to more available oxidizing species, while lower concentrations slow these processes. Sapountzi et al. showed that higher $FeCl_3$ concentrations resulted in faster deposition rates and more uniform coatings of polypyrrole (PPy) onto PAN nanofibers and vice versa[23]. With low $FeCl_3$ concentrations, the limited availability of oxidizing species slows down the formation of radical cations and the subsequent polymerization process[25,26]. On the other hand, Xue et al. reported that an optimal $FeCl_3$ concentration of 0.25 M resulted in a uniform and highly conductive PPy coating onto PAN nanofibers, while higher concentrations led to over-oxidation and degradation of the polymer[27]. Wissmann et al. studied the deposition of polyaniline (PANI) onto PAN nanofibers and observed that increasing the $FeCl_3$ concentration from 0.1 M to 0.5 M significantly increased the deposition rate and conductivity of the PANI coating, but further increasing the concentration resulted in non-uniform deposition. Zhang et al. reported the deposition of a copolymer of aniline and *o*-anisidine onto PAN nanofibers using different $FeCl_3$ concentrations. They found that an optimum $FeCl_3$ concentration of 0.25 M resulted in a uniform and highly conductive coating, while higher concentrations led to over-oxidation and degradation of the polymer, as identified by the lower conductivity of the material[28]. Thus, careful selection of oxidant concentrations is critical to ensure optical EAP coatings.

This research demonstrates the use of CVD for the preparation of poly(3,4-ethylenedioxythiophene) (PEDOT)-coated PAN nanofibers. This research thus focuses on the process which involves electrospinning PAN nanofiber initially, followed first by infusing these PAN nanofibers with $FeCl_3$ at various concentrations and then by the deposition of EAPs onto the $FeCl_3$-ladden fibers, as shown in **Figure 1**. The study explores the influence of different concentrations of $FeCl_3$ on the deposition rate of PEDOT onto the nanofibers. Mechanical testing assesses the effect of PEDOT coatings on the mechanical properties of the materials, particularly in high-humidity environments indicative of the material's pertinency to biomedical and water purification applications. The optimization of $FeCl_3$ concentration is pivotal to ensuring efficient and precise deposition of EAPs, leading to uniform coatings and improved material properties. The absence of comprehensive studies examining the effects of $FeCl_3$ concentrations and VPD setup characteristics on the deposition rate and functionality of EAP-coated PAN nanofibers underscores the significance of this research. The results of this work are especially significant given the differences observed in the EAP deposition at lower $FeCl_3$ concentrations compared to previous studies, highlighting the critical role of the vapor phase deposition (VPD) setup.

Protocol

1. Experimental setup

1. Electrospinning of PAN nanofibers
    1. Dissolve 1 g of PAN in 10 mL of DMF to create a 10% solution.

2. Assemble the electrospinning setup, ensuring that the high-voltage power supply, syringe pump, and a 20-gauge needle with a flat tip are connected to a grounded collector shown in **Figure 1** and **Figure 2**. Ensure that the electrospinner is used in a fume hood or connected to ventilation ducting to minimize exposure to solvent vapors.
3. Cover the metal collection drum, which will receive the polymer nanofibers, with wax paper for easy fiber retrieval and minimal cross-contamination between samples.
4. Fill the syringe with the PAN solution and connect it to the spinneret needle using a 0.8 mm ID polytetrafluorethylene (PTFE) tube with Luer adapters.
5. Set the flow rate of the syringe pump to 0.04 mL/min. The flow rate can be adjusted as needed depending on the polymer solution properties.
6. Apply a voltage of 18.9 kV between the spinneret and the grounded collector, which is set to rotate at 1,200 rpm[29,30]. Follow proper guidelines during electrospinning as the process involves high voltage.
7. Allow the charged jet to initiate from the spinneret, where it solidifies into continuous nanofibers as the solvent evaporates. Ensure that the applied voltage, solution flow rate, and drum rotation speed are consistent across all batches to achieve uniform fiber morphology and diameter.
8. Allow the PAN nanofibers to deposit on the grounded collector coated with wax paper for approximately 4.5 h. After this time period, unwrap the wax paper from the drum by removing the tape.

2. Preparation of PAN coupons
    1. Dry the PAN sheet mat in a vacuum desiccator at room temperature for 72 h to remove any residual solvent or water adsorbed during processing.
    2. Cut the dried fiber mats into 2 cm x 2 cm coupons with scissors or a razor blade. Note the positions of the coupons with respect to the direction of drum rotation, as shown in **Figure 3**. Organize coupons into groups of triplicates, producing replicates from the same column of the fiber mat to ensure consistency.
3. Vacuum system assembly
    1. Assemble the chemical vapor phase deposition system using an enclosed steel container with a glass lid fitted with a silicone gasket to precisely control vacuum conditions, as shown in **Figure 4**.These containers are commercially available as vacuum degassing chamber kits from a variety of vendors and are inexpensive.
    2. Equip the system with two valves to manage the vacuum: one valve connects to the vacuum pump and is closed once the desired vacuum is reached; the other valve connects to the atmosphere and is opened to allow controlled release of the vacuum as needed.
    3. Connect a vacuum pump to the system to reduce the pressure in the chamber. Position the container on a hot plate capable of reaching temperatures up to 250 °C to enable thermal management during the deposition process.
4. Vapor phase deposition rack assembly

1. Develop deposition racks for the project as per the designs for two deposition rack designs described below.
2. Construct the Generation 1 (G1) deposition rack shown in **Figure 5A** by wrapping four vertical legs made of stainless steel in aluminum foil to prevent contamination.
3. Connect the vertical legs with horizontal rods at the top and bottom, forming a hollow cube-like structure for stability.
4. Wind three horizontal copper wires around the legs to create three tiers or levels for hanging the coupons.
5. Ensure that the G1 rack is compact, fits within a processing chamber, and allows for easy assembly and disassembly.
6. Construct the Generation 2 (G2) setup, shown in **Figure 5B**, using stainless steel for durability and corrosion resistance. Engineering schematics for this system are provided in **Supplementary File 1**. Design the G2 rack with a circular base and top plate connected by four vertical rods for stability and support. Equip the vertical rods with adjustable clamps to allow customization of the height between the base and top plate. Install a circular wire mesh tray made of stainless steel for hanging coupons.
7. Ensure precise control over the positioning of electrospun coupons during the deposition process to promote uniform exposure to the vapor phase.

2. Vapor phase deposition

1. Deposition of $FeCl_3$ on PAN coupons
    1. Weigh the PAN coupons. Deposit $FeCl_3$ (oxidant) on the PAN coupons (at least three replicates per condition) by soaking them in aqueous $FeCl_3$ solutions of varying concentrations, ranging from 1 M to 5 M, for 30 min.
    CAUTION: Exercise caution when handling ferric chloride (anhydrous), as it is a corrosive irritant that can cause severe eye damage.
    2. Transfer the coupons onto low-lint paper wipes to facilitate osmotic drying, replacing the wipes 2x.
    3. Wrap the coupons in wipes and place them inside a fume hood for 24 h to complete the first stage of the drying process.
    4. Weigh the PAN coupons after 24 h and record the weight loss. Hang the PAN coupons by hooking them onto the metal wire tray prepared in step 1.4.9.
    5. Place a 500 mL beaker containing dry calcium chloride desiccant at the bottom of the setup. Position the entire setup inside a vacuum chamber.
    6. Initiate the vacuum by turning on the pump and leaving the vacuum valve open for continuous air removal, effectively using the vacuum system as a desiccator. Here, the pumping rate was 85 L/min. The final vacuum achieved by this pump and setup was approximately 8000 Pa.
    7. Monitor the weight loss of the coupons at intervals of 1 h, 2 h, 3 h, 24 h, 48 h, and 72 h.
2. PEDOT deposition onto PAN coupons
    1. Hook and hang the PAN coupons on the coupon rack assembly.
    2. Suspend the coupons inside the vacuum system along with an open glass container holding

approximately 4 g of the monomer (EDOT). Adjust the hot plate temperature to 55 °C.

3. Open the valve between the chamber and the vacuum pump and evacuate the chamber until the desired vacuum (8000 Pa) is achieved. Then, close the valve, leaving the chamber under vacuum.
4. Allow the vapor deposition process to occur for 2 h. After 2 h, open the vacuum release valve to retrieve the PEDOT-coated coupons.

3. Coupon washing
    1. Remove the polymer-coated coupons from the VPD chamber and transfer them to the washing chamber.
    2. Place the coupons over the opening of a porcelain funnel lined with circular filter paper of 5.5 cm in diameter and a pore size of 180 µm, as shown in **Figure 6**.
    3. Wash each batch of three coupons of a specific concentration together to remove $FeCl_3$ residue by spraying methanol over the coupons using a squirt bottle.
    4. Ensure thorough removal of $FeCl_3$ residue by increasing methanol volume with higher concentrations to effectively dissolve and wash away residual oxidant and monomer. Use approximately 200 mL of methanol for coupons dipped in 1 M $FeCl_3$. Increase the methanol amount by 50 mL for each higher concentration level (e.g., 250 mL for 2 M, 300 mL for 3 M).
    5. After washing, leave the coupons to dry under the hood for 30 min followed by drying in a desiccator with desiccant at room temperature for 1 h and finally preserve them in glass vials.
4. Cleaning of the VPD chamber and pump
    1. Rinse the CVD chamber with acetone to dissolve the unreacted monomer. Dispose of the rinse in the organic waste container.
    2. Place the chamber in a fume hood while empty and heat it at 30 °C for 1 h. Immerse the chamber in a detergent solution for 24 h and then dispose of the detergent.
    3. Heat the chamber with the lid slightly open at 200 °C for 24 h. Perform another round of acetone spraying and dry the chamber in the fume hood at 30 °C for 1 h.
    4. Change the pump oil after each batch of monomer deposition to maintain the integrity of the experiment.

3. Characterization of samples

1. SEM analysis of nanofiber mat
    1. Attach PAN, PAN+$FeCl_3$, and PAN+$FeCl_3$+PEDOT samples to aluminum stubs using carbon tape.
    2. Image the samples at a magnification of 5000x, using a spot size of 4.5 nm and an accelerating voltage of 20 kV. Adjust imaging parameters as necessary to investigate sample morphology.
    3. Use the measurement function to determine fiber diameters. Take 12-15 measurements for a sample.
    4. Perform energy dispersive X-ray spectroscopy (EDS) analysis according to the standard operating procedures of the SEM instrument. Obtain the atomic percentage and weight percentage of the elements found in the samples.
2. Mechanical analysis

1. Laser cut 40 mm x 40 mm cardboard frames with 20 mm x 20 mm centered window openings.
2. Using a razor blade, precisely cut out 10 mm x 40 mm nanofiber sample strips with the 40 mm edge being parallel to the direction of electrospun nanofiber formation.
3. Measure the thickness (mm) of each strip using digital calipers at five locations chosen around the center of the specimen where the sample would not be in contact with the frame and about equal distances apart. Take the average as the thickness. Measure the weight (g) of each strip.
4. Condition the sample either by desiccation (vacuum desiccator filled with calcium sulfate) or soaking in phosphate-buffered saline (10x PBS) for 72 h.
5. Dab PBS-soaked samples on lint-free tissue wipes. Overlay a 10 mm x 40 mm polymer sample onto a 40 mm x 40 mm frame and tape it down for insertion into the tensile tester.
6. Load the frame and sample into the tensile tester and test at room temperature and the desired strain rate (0.8 s^{-1}). The output will be in force and displacement.
7. Convert the force and displacement into stress-strain. Calculate the density of the sample from the sample dimensions and mass. To calculate stress, divide the force data collected by the tensile tester by the sample's cross-sectional area, then multiply by both the density of the fiber mat and the gauge length used while testing.

Representative Results

In this work, electroactive polymer-coated PAN nanofibers are fabricated by electrospinning to develop highly porous yet strong materials that could be used as filters, absorbents, and photocatalysts for water purification, substrates for electrocatalysis, and scaffolds/matrices for tissue engineering, nerve regeneration, drug delivery, and biosensing. To provide these materials with electroactive properties, PAN nanofibers are coated with the EAP PEDOT by chemical vapor deposition.

The formation of the coupons began by electrospinning PAN solutions, resulting in the formation of white, homogenous nanofiber mats. After electrospinning, the PAN nanofiber mats were dried in a vacuum desiccator for 72 h to remove any residual solvent or water. The dried nanofiber mats were then cut into 2 cm x 2 cm coupons using scissors, ensuring that the positions of the coupons were noted according to the direction of the drum rotation, as shown in **Figure 3**. In this way, it was possible to determine whether coupon position impacted morphology. The resulting nanofiber mats were uniform in appearance, with a consistent white color and homogeneity in terms of weight along the direction of the drum rotation. Coupons were organized into groups of triplicates, with replicates taken from the same column of the fiber mat, further ensuring consistency in thickness and appearance across all samples.

The first step in the coating of the PAN nanofibers with the EAP is the application of $FeCl_3$, which acts as an oxidant enabling the polymerization of EDOT vapors into PEDOT coatings. The investigation into the drying of $FeCl_3$-soaked PAN coupons, with $FeCl_3$ concentrations ranging from 1 M to 5 M, is shown in **Figure 7A**. Fresh, uncoated coupons originally had an average weight of 10.6 ± 1.1 mg. For all samples, a gradual decrease in mass occurred with time, eventually leveling off after 72 h. **Figure 7B** illustrates the percentage of weight gain for electrospun PAN mats deposited with $FeCl_3$ at various concentrations, increasing from 146% at 1 M to 400% at 5 M. In general, increased $FeCl_3$ concentration led to an increase in the weight gain of the coupons, suggesting higher absorption of $FeCl_3$ onto the nanofiber mats.

After oxidant deposition, the next step of the process is EAP growth by VPD. **Figure 8A** shows the percentage weight increase of the PAN coupons through the PEDOT deposition process with varying $FeCl_3$ concentrations (1 M to 5 M). The increase in coupon weight during deposition was measured at two stages: (1) VPD of PEDOT on $FeCl_3$-coated PAN coupons before washing (sample labeled PAN+PEDOT), and (2) VPD of PEDOT on $FeCl_3$-coated PAN coupons where the coupons were washed with methanol to remove $FeCl_3$ and dried after deposition(sample labeled PAN+PEDOT+Wash). The results revealed that the percentage of weight gain during the initial VPD of PEDOT increased with $FeCl_3$ concentration, from 142% at 1 M to 470% at 5 M. When the coupons were washed after PEDOT deposition, the observed weight was lower, ranging from 73% at 1 M to 267% at 5 M, due to the removal of iron salts (both $FeCl_2$ that is the product of the oxidation reaction and unreacted $FeCl_3$) and unreacted EDOT. These outcomes underscore the critical role of $FeCl_3$ concentration in enhancing polymer deposition and retention, indicating that higher $FeCl_3$ concentrations improve initial deposition while the washing step selectively removes unbound components.

Table 1 provides the average fiber diameters, and **Figure 8B** delineates the percentage increase in the diameter of PAN nanofibers through two stages of PEDOT deposition with varying $FeCl_3$ concentrations. **Figure 9** and **Supplementary File 2** provide representative SEM images of these samples at high and low magnification, respectively. In the first stage, where the coupons are not washed post-PEDOT deposition, the diameter increase significantly rises from 36.4% at 1 M $FeCl_3$ to 156.1% at 3 M but cannot be measured with 4 M and 5 M $FeCl_3$ due to inter-fiber bridging caused by the high concentration of $FeCl_3$ and extensive PEDOT deposition. In the second stage, after washing, the diameter increase is notably lower, ranging from 10% at 1 M $FeCl_3$ to 97% at 5 M, demonstrating how higher $FeCl_3$ concentrations enhance initial polymer growth but also showing the effect of washing in removing iron salts and unreacted EDOT. These results highlight the importance of $FeCl_3$ concentration in influencing the degree of polymer deposition and the structural integrity of the nanofibers, with higher concentrations leading to greater diameter increases but also posing challenges due to fiber bridging.

Figure 10 illustrates the EDS spectra of PAN fibers and their composites with $FeCl_3$ and PEDOT; distinct differences in elemental composition can be seen. The EDS spectrum of pure PAN fibers (**Figure 10A**) displays prominent peaks corresponding to carbon, nitrogen, and oxygen, which are characteristic of PAN. **Figure 10B** presents the EDS spectrum of PAN fibers soaked in 3 M $FeCl_3$, revealing additional peaks for iron and chlorine alongside the PAN-related elements. This indicates the incorporation of Fe and Cl from $FeCl_3$ onto the fiber structure. Lastly, in **Figure 10C**, the EDS spectrum of PAN+PEDOT+Washed fibers synthesized with 3M $FeCl_3$ is shown where, in addition to the PAN elements, sulfur (S) from PEDOT and residual Fe and Cl from the iron salts are observed. These data are also supported by **Supplementary Table 1**, which details the elemental composition of PEDOT-coated nanofibers as a function of increased $FeCl_3$ used for vapor phase polymerization of the EAP. The presence of Fe and Cl suggests incomplete removal of iron salts during the washing process. Note that even if residual iron salts were completely removed from the fibers, chloride ions would still be present as bound counterions to the doped PEDOT. The comparison across these spectra highlights the gradual incorporation of additional elements as the fiber synthesis process incorporates iron, chlorine, and PEDOT.

Figure 10D demonstrates the sulfur content in PEDOT-deposited PAN nanofibers across different concentrations of $FeCl_3$, ranging from 1 M to 5 M, as determined from EDS analysis. The data reveals a clear trend where the ratio of sulfur (from PEDOT) to nitrogen (from PAN) increases with higher $FeCl_3$ concentrations, as depicted by the blue bars. This upward trend in the sulfur/nitrogen ratio suggests that increasing the concentration of $FeCl_3$ enhances the efficiency of PEDOT deposition onto PAN nanofiber mats, likely due to more effective oxidative polymerization of EDOT. The standard deviation, represented by the vertical lines, shows slight variability across different concentrations but remains relatively consistent, indicating reproducibility in the PEDOT deposition process.

Mechanical testing of the nanofiber mats was conducted to investigate the potential of these materials in a variety of applications that would require their use in the dry (solar energy collection) or wet (biomedical, water purification) state. Evaluation of the nanofibers in the wet state was conducted in phosphate-buffered saline solutions that mimic the physiological fluids that would be encountered in wound healing, tissue engineering, biosensing, and drug delivery applications. A representative stress-strain plot is shown in **Figure 11A**, demonstrating the uniaxial tensile response of various electrospun PAN nanofibers samples, focusing on the mechanical differences between desiccated and PBS-soaked samples. For the dried uncoated PAN fiber mats, the measured elastic modulus, ultimate tensile strength, and toughness are within the range that has been measured for PAN fiber mats in the literature (**Figure 11B**)[31]. As previously mentioned, to coat the samples with PEDOT, the PAN is soaked in a $FeCl_3$, which acts as a plasticizer in the mat, decreasing the modulus and ultimate tensile strength and increasing the ductility of the film (**Figure 11A**). Once the PEDOT is deposited and the $FeCl_3$ is washed away with methanol, the mechanical properties of the dried fiber mats are recovered, in which the PEDOT coating does not have a significant impact on the mechanical properties (**Figure 11B**). Researchers have previously demonstrated that coating a PEDOT: polystyrene sulfonate(PSS) coating on an electrospun PAN fiber mat slightly increases the elastic modulus but has no significant impact on the ultimate stress[32]. We hypothesize that the difference in the impact of the coating on the elastic modulus between the literature and our results could be due to the PSS. Through these measurements, we observed that hydration has the largest impact on the mechanical response of PAN, significantly decreasing all three mechanical properties measured when the pure PAN nanofibers were soaked in PBS. However, we

do observe that the PEDOT coating partially mitigates the impact of hydration on the ultimate strength, toughness, and modulus of the PAN nanofibers, as PEDOT has been shown to be insoluble in water[33].

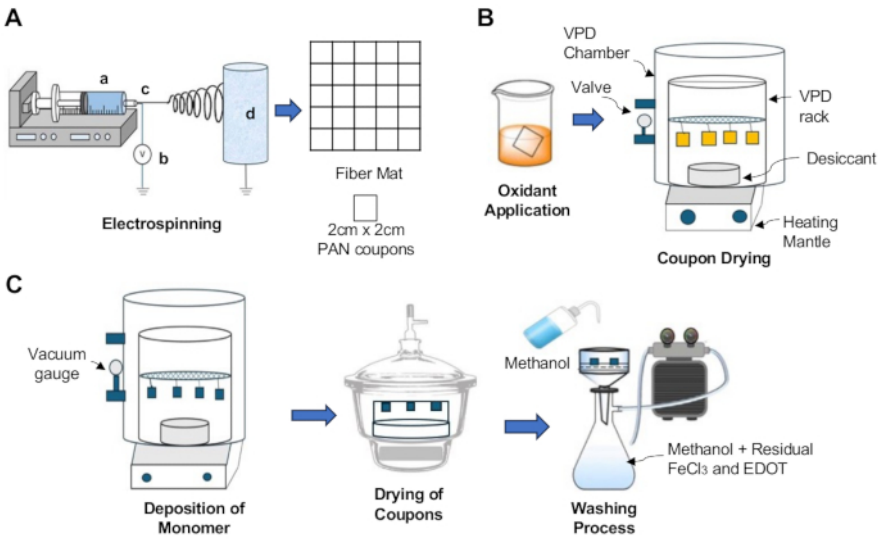

Figure 1: Graphical representation of the process of preparation of PEDOT-coated PAN nanofibers. (**A**) Components of electrospinner: (a) Liquid feeding system where a syringe pump delivers the polymer solution at controlled rates. (b) Power source with high voltage supply (up to +50 kV) that polarizes the emitter and collectors. (c) Spinneret (conductive needle or extrusion tube), which affects fiber structure. (d) Drum collector. (**B**) Process of soaking PAN nanofiber coupons with $FeCl_3$ oxidant, followed by drying. (**C**) Process of coating of PAN nanofibers with PEDOT by vapor phase oxidative polymerization of EDOT monomer followed by washing and drying. Please click here to view a larger version of this figure.

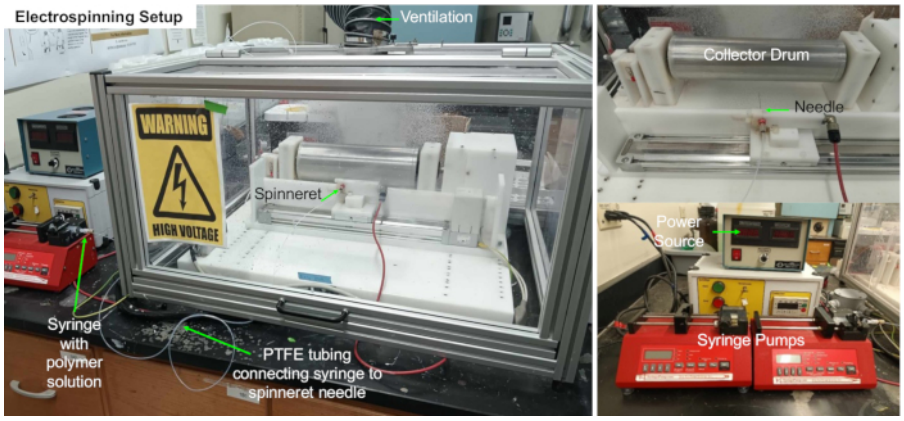

Figure 2: PAN nanofiber preparation. Photograph of the experimental setup showing the electrospinner used for this experiment. Note that the box around the electrospinner is equipped with a safety interlock so that the high voltage can only be supplied when the box is closed, reducing the risk of electric shock. The box is also connected to an exhaust snorkel to minimize exposure to solvent vapors. Please click here to view a larger version of this figure.

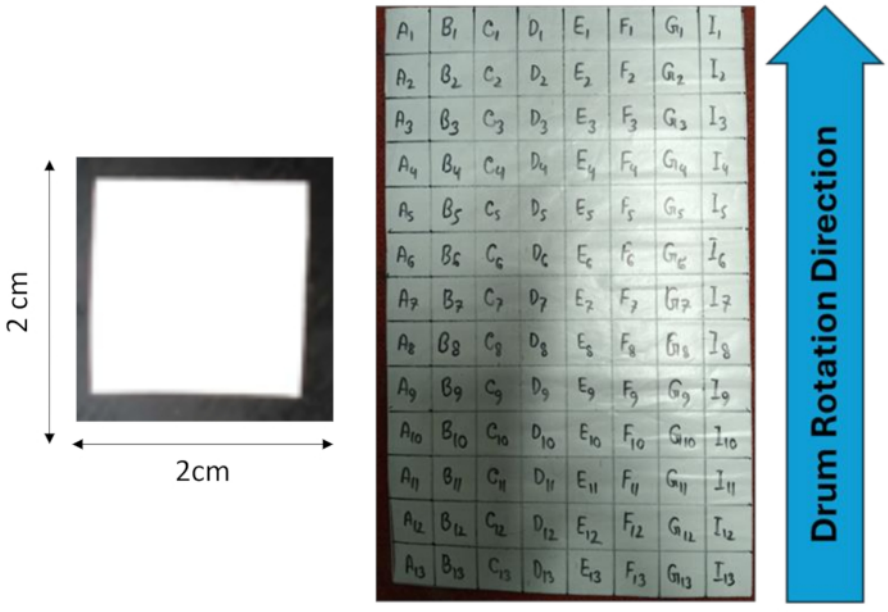

Figure 3: Preparation of PAN coupons. Grid layout for PAN nanofiber coupon preparation. A 13 x 8 matrix yields 104, 2 x 2 cm coupons. Note that the coupon labels are written on a piece of wax paper placed over the fiber mat for illustration purposes only; there was no writing on the coupons themselves. Please click here to view a larger version of this figure.

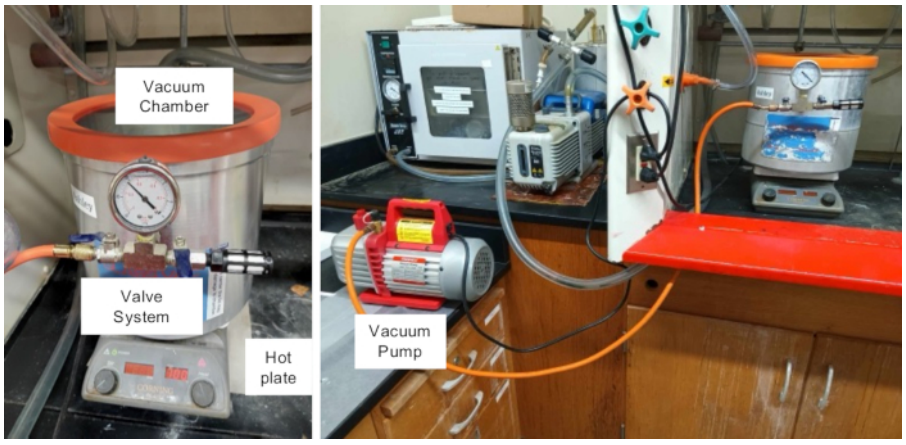

Figure 4: Vacuum deposition system assembly. Photograph of the experimental setup showing the vacuum chamber (an inexpensive stainless steel commercial degassing chamber with glass/silicone lid), valve system, vacuum pump, and hot plate. Please click here to view a larger version of this figure.

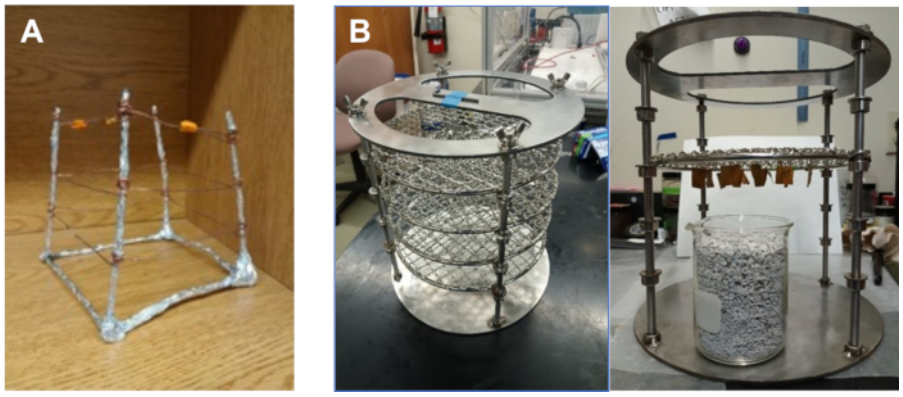

Figure 5: Photographs of the deposition racks used for processing PAN coupons. (**A**) G1 and (**B**) G2 protopyes of these racks. Racks were designed to fit inside the vacuum chamber shown in **Figure 4**. Please click here to view a larger version of this figure.

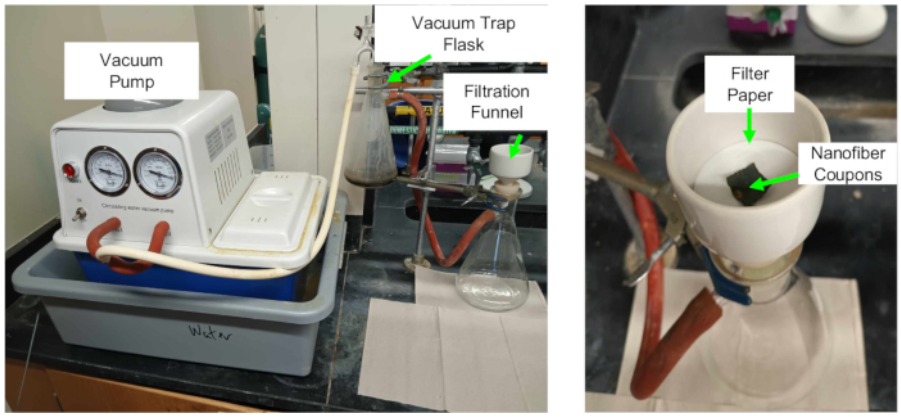

Figure 6: Photograph of the vacuum filtration apparatus used for coupon washing. Please click here to view a larger version of this figure.

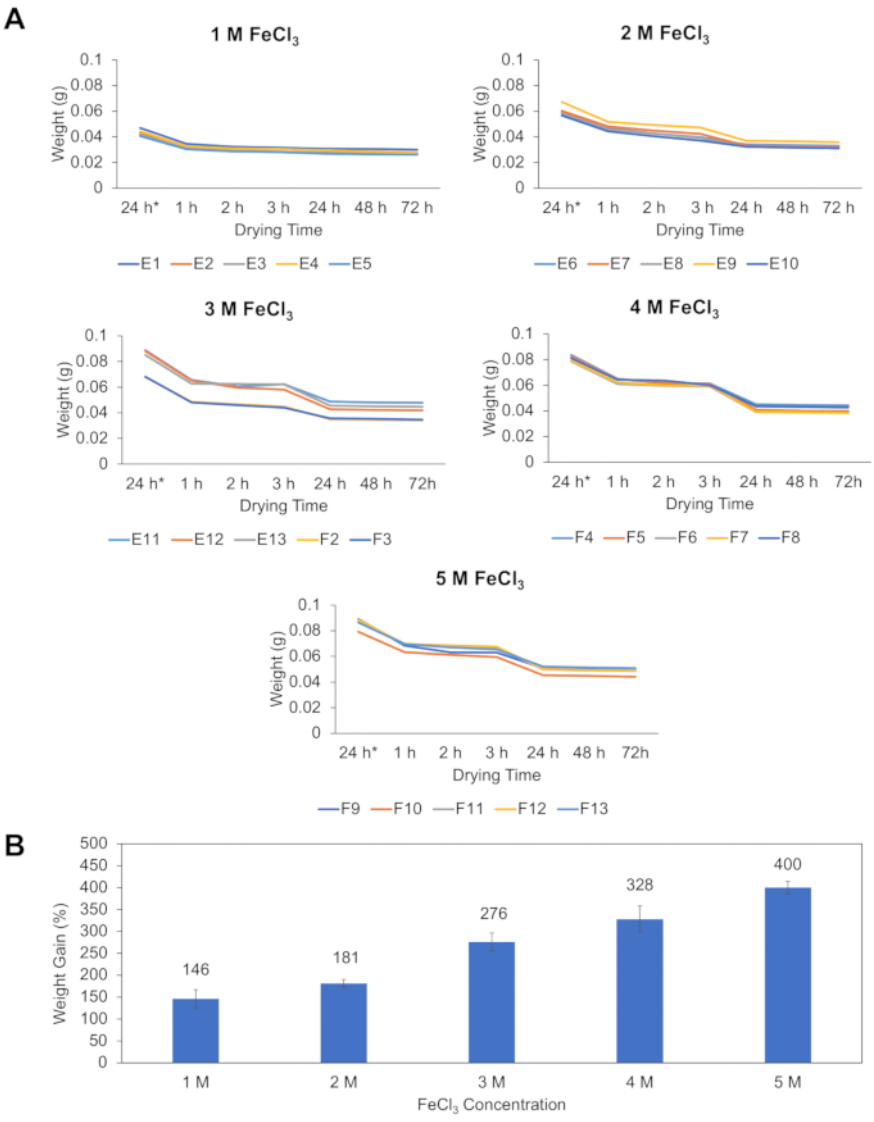

Figure 7: Effect of drying process on weight of PAN coupons after deposition of $FeCl_3$. (**A**) Weight changes of $FeCl_3$-soaked PAN coupons during the drying process. The y-axis represents the sample weight (g), while the x-axis denotes the drying time. For each $FeCl_3$ concentration, the drying time is divided into five stages: Stage 1 (indicated with an *) represents 24 h of hood drying, while stages 2 - 7 represent 1, 2, 3, 24, 48 and 72 h, respectively, in a desiccator under vacuum. The sample names (E1 - F8) represent the source location of the coupon within the nanofiber mat grid. (**B**) Percent weight gain of PAN nanofiber coupons upon soaking with varying $FeCl_3$ concentrations and drying. The vertical axis represents the percentage increase in sample weight relative to the original PAN fiber, while the horizontal axis represents the $FeCl_3$ concentration. Error bars represent the standard deviation between replicates (n = 5). Please click here to view a larger version of this figure.

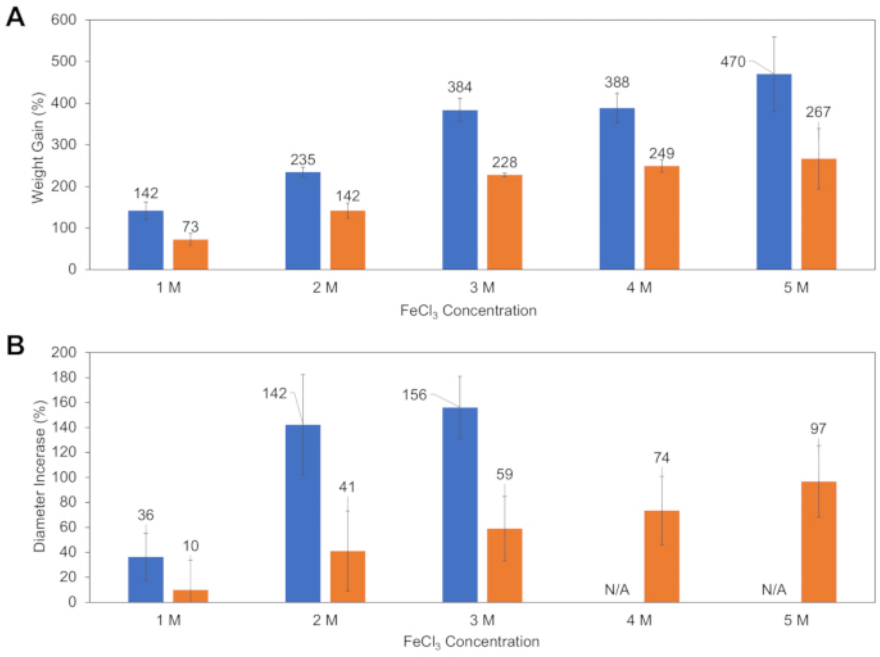

Figure 8: Effect of PEDOT deposition on PAN nanofibers. (**A**) Percent weight gain and (**B**) percent increase in diameter for PEDOT deposition on PAN coupons with varying $FeCl_3$ concentrations (1 M to 5 M), measured after initial deposition (PAN+PEDOT, blue) and post-washing with methanol (PAN+PEDOT+Wash, orange). Error bars represent the standard deviation between replicates (n = 3). Diameter increase was not measurable with 4 and 5 M $FeCl_3$ due to inter-fiber bridging because the $FeCl_3$-coated fiber diameters increased so much that they grew together. Please click here to view a larger version of this figure.

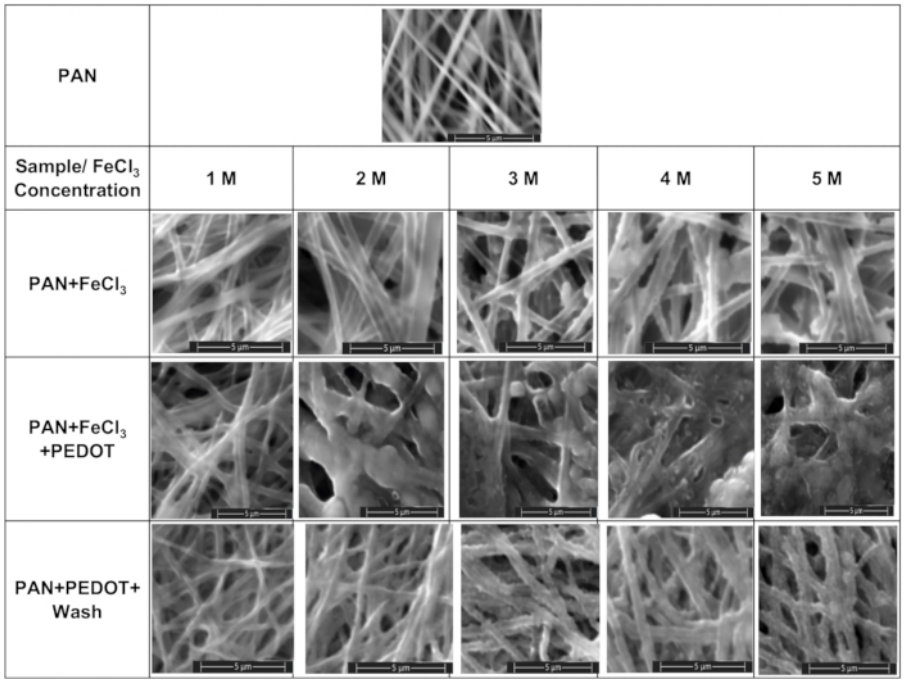

Figure 9: Representative scanning electron microscopy (SEM) images of bare and treated PAN nanofiber mat samples. Please click here to view a larger version of this figure.

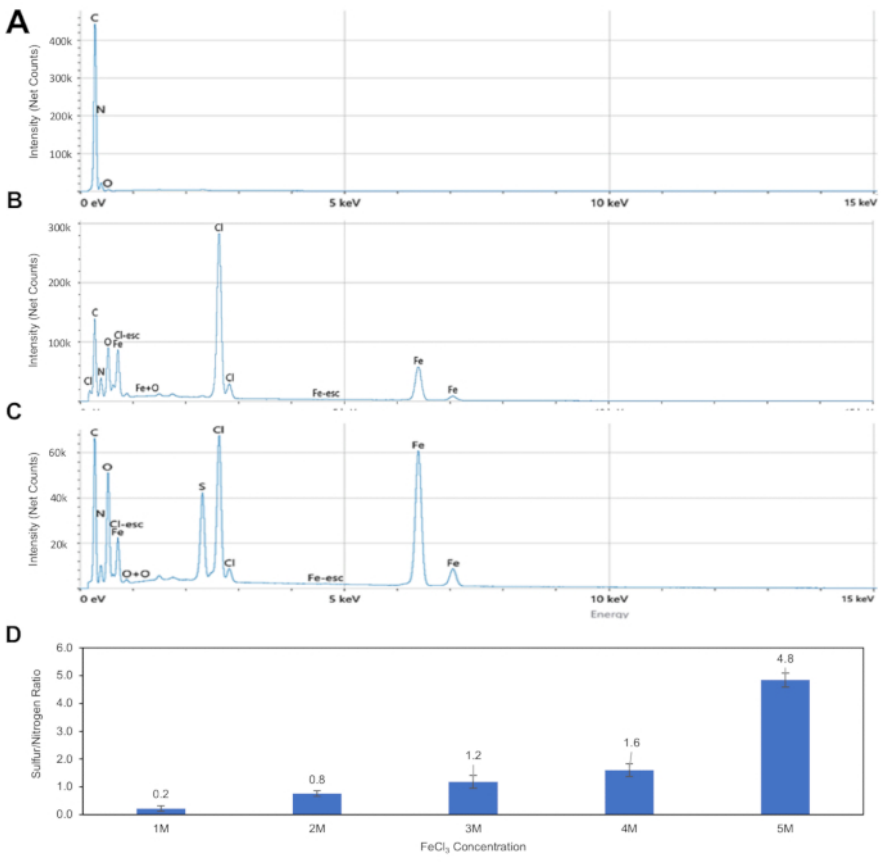

Figure 10: Changes in composition of PAN nanofibers as a result of the coating process. EDS spectra of (**A**) PAN fibers, (**B**) PAN fibers soaked in 3 M $FeCl_3$ and dried, and (**C**) PAN+PEDOT+Wash fibers prepared with 3M $FeCl_3$ after washing and drying showing elemental peaks corresponding to C, N, and O from PAN, Fe and Cl from $FeCl_2$/$FeCl_3$, and S from PEDOT. The horizontal axis (X-axis) represents the energy of the detected X-rays in kiloelectron volts (keV) corresponding to the characteristic energy levels of the elements in the sample. The vertical axis (Y-axis) represents the intensity of X-ray counts, indicating the relative abundance of each detected element. (**D**) Sulfur/nitrogen ratio on PAN nanofiber mats after PEDOT deposition and washing from EDS analysis for samples treated with varying concentrations of $FeCl_3$ (1 M to 5 M). Error bars represent the standard deviation between replicates (n = 3). Please click here to view a larger version of this figure.

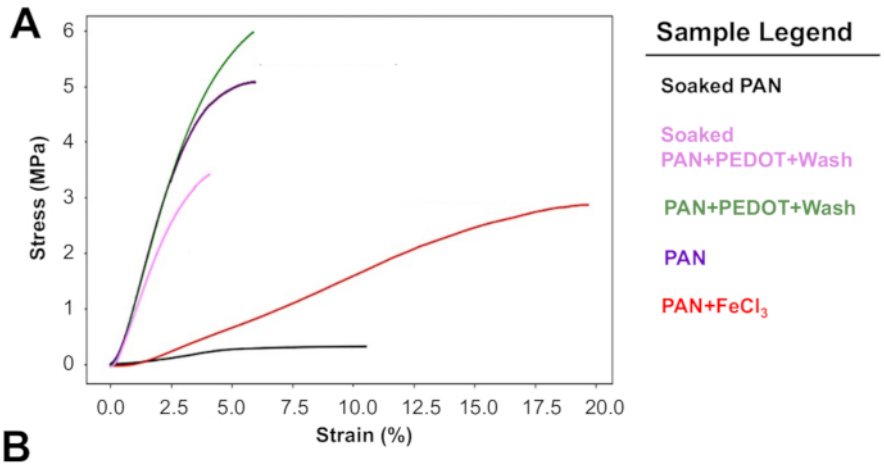

Figure 11: Mechanical Properties of Nanofiber mats. (**A**) Representative stress-strain responses of five nanofiber samples subjected to differing post-treatment processes. (**B**) The Young's modulus, ultimate strength, and toughness of the samples depend on post-treatment processes. The black curve represents pure polyacrylonitrile (PAN) nanofibers that were soaked in a phosphate-buffered saline (PBS) solution for 72 h. For both parts of the figure, the dark purple dataset represents pure PAN nanofibers that have been desiccated (n = 12). The black dataset represents pure polyacrylonitrile (PAN) nanofibers that were soaked in a phosphate-buffered saline (PBS) solution for 72 h (n = 6). The green dataset represents PAN that was coated with PEDOT using ferric chloride as an oxidant and then desiccated before mechanical analysis. The light purple dataset represents PAN that was coated with PEDOT using ferric chloride as the oxidant and then soaked in a PBS solution before mechanical analysis (n = 3). The red dataset represents PAN that has been soaked in the ferric chloride oxidant (n = 5). All error bars indicate standard error. Please click here to view a larger version of this figure.

	PAN+$FeCl_3$+PEDOT		PAN+PEDOT+Wash	
$FeCl_3$ Concentration	Average Fiber Diameter (nm)	Std. Dev.	Average Fiber Diameter (nm)	Std. Dev.
1 M	482	67.2	389	83
2 M	856	142.1	499	113
3 M	905	88.4	562	91
4 M	0	0	613	97
5 M	0	0	695	101

Table 1: Diameter of nanofibers after initial PEDOT deposition (PAN+$FeCl_3$+PEDOT) and post-washing (PAN+PEDOT +Wash) as a function of $FeCl_3$ oxidant concentration used (n = 5 to 12).

Supplementary File 1: Deposition hanger engineering drawing. Please click here to download this file.

Supplementary File 2: Representative low magnification scanning electron microscopy (SEM) images of PEDOT-coated PAN nanofiber mats. Please click here to download this file.

Supplementary Table 1: Elemental composition of PAN+PEDOT+Wash samples prepared with varying $FeCl_3$ oxidant concentrations determined from EDS analysis. Please click here to download this table.

Discussion

In this work, protocols for electrospinning nanofiber mats from commodity polymers, coating these nanofibers with electroactive polymers by vapor phase oxidative polymerization, and characterization of the chemical and mechanical properties of these materials are described.

Electrospinning has become a useful tool for the generation of high surface area materials for a range of applications from biomedicine to sustainability and electronics[1,2]. Considering the high voltage required for electrospinning, purchasing from a specialized system from a reputable brand is advisable. Having said that, readers are referred to external resources that discuss best practices for building electrospinning systems[34]. The properties of electrospun materials are controlled by numerous polymer solutions and process variables. Key parameters such as viscosity, concentration, conductivity, molecular weight, and surface tension of the polymer solution used for electrospinning affect fiber formation and diameter[35,36,37,38,39,40]. In general, polymers with higher molecular weight and flexibility tend to form more entangled networks, crucial for stable fiber formation and mechanical strength. Intermolecular interactions like hydrogen bonding and van der Waals forces further promote chain entanglement. Polymer solution concentration has a direct correlation with the diameter of electrospun nanofibers. Similarly, process parameters, including applied voltage, flow rate, syringe positioning

relative to the collector drum, tip-to-collector distance, temperature, relative humidity, and electrical potential, and syringe needle type, diameter, and shape also affect the properties of electrospun nanofibers. The collector's distance from the needle determines the solvent evaporation extent, and the collector's rotation speed determines the extent of nanofiber alignment[36]. Applied voltage has been shown to be inversely proportional to fiber diameter, while fiber uniformity and alignment are directly proportional to voltage and collector drum rotational speed, respectively[41,42]. As the rotation speed of the drum collector increases, the fibers experience greater tensile forces during deposition, promoting alignment along the drum's axis. At lower speeds, such as 1,200 rpm used in this study, the fibers tend to deposit randomly, forming a nonwoven mat. For enhanced alignment, drum speeds in the range of 3,500-4,000 rpm are typically required. The specific parameters specified in this protocol (polymer solution concentration, injection rate, voltage, and drum rotation speed) will likely need to be optimized for the particular setup available. In addition, because different applications benefit from different material properties, process parameters will also need to be adjusted to obtain the desired base nanofiber architecture. Alignment, for example, is particularly desirable for applications requiring anisotropic properties, such as in the development of scaffolds for tissue engineering or applications requiring directional conductivity for electronic materials.

The described method for coating the electrospun mats with EAPs by VPD is adaptable and relatively easy to set up in various laboratories. Compared to other coating techniques like electrodeposition and dip-coating, this VPD approach offers significant advantages. VPD allows for uniform, thin coatings with minimal solvent use, making it an eco-friendly and accessible option for non-conductive substrates[43]. The method's reliance on standard lab equipment further broadens its accessibility, while the ability to control coating thickness and composition precisely supports the development of mechanically robust, conductive nanofibers suitable for various research applications. VPD outcomes depend on the types and concentrations of monomers, oxidants, and substrates, as well as critical operational parameters like vacuum level, temperature, and exposure time[23,43]. One of the critical steps enabling VPD of EAPs onto nanofiber mats is the deposition of the $FeCl_3$ oxidant, which requires precise control over concentration to ensure uniform distribution and enable uniform polymerization. Vacuum and increased temperatures promote volatilization of the monomer to enable its deposition at the nanofibers' surface. As such, these are additional parameters that can be optimized for the deposition of various EAPs. The VPD system utilized in this work enabled the investigation of the effect of $FeCl_3$ concentration on the EAP deposition onto PAN coupons. Specifically, the increased weight gain, increased nanofiber diameter, and increased sulfur content of the fibers upon VPD using $FeCl_3$ oxidant concentrations from 1 M to 5 M clearly indicates that the concentration of oxidant used is critical to facilitate and control PEDOT deposition on the nanofibers. Excessive PEDOT deposition can, in certain applications, be detrimental. For example, excessive coating with the EAP may significantly reduce transport properties through the material or mask fiber alignment that may have been required for certain tissue engineering applications.

Another critical step in the protocol is that of washing the coupons after EAP deposition to remove unreacted $FeCl_3$ and electroactive monomers, which, if left on the fibers, could reduce material performance[24,27]. In our results, EDS spectral analysis showing the presence of Fe and Cl provided evidence of the presence of residual $FeCl_3$ on

the nanofibers, even after washing. In particular, EDS data showed that residual Fe content correlated with the concentration of $FeCl_3$ used for oxidative polymerization of the EAP (**Supplementary Table 1**). This is a limitation of the procedure that could potentially affect the nanofiber's functionality in particular applications. As such, careful timing and handling during both deposition and washing are vital for maintaining the purity and consistency of the final material[23,27]. When $FeCl_3$ clustering is observed, adjustments such as the application of a more controlled deposition method can improve coating uniformity. Optimizing VPD process conditions such as vacuum level and exposure time can further enhance coating uniformity. Additionally, maintaining precise temperature settings during VPD can control PEDOT growth rates, preventing excessive polymer accumulation that could lead to fiber bridging and compromise coating uniformity[28]. When required, more extensive washing protocols can be utilized that involve soaking steps or the use of other solvent systems.

With respect to the nanofiber characterization, another limitation of the procedure specified in this work is the examination of samples via SEM without the use of sputter coating. The main challenges associated with imaging of polymeric samples by SEM include charge buildup that causes charging on the sample surface and can distort image quality, as well as sensitivity to electron beam and high vacuum, which can result in damage to the sample's architecture[44]. Sputter coating with a few nanometers of a conductive material like carbon, iridium, gold, or platinum can minimize sample charging and damage by providing a mechanism for electron dissipation[45]. Alternatively, the use of low-voltage SEM techniques or SEM imaging using back-scattered electron detectors are alternatives that can result in enhanced image clarity[44,45].

The analysis of mechanical properties, particularly the uniaxial tensile strength, provides insight into the functional benefits of PEDOT deposition. The observed increase in tensile strength in soaked PEDOT-coated samples compared to pure PAN nanofibers suggests that the electroactive polymer contributes to enhanced mechanical stability under hydrated conditions. This enhancement is particularly significant in environments with high humidity like in biomedical applications, as indicated by the PBS-soaked samples, where the PEDOT coating provides substantial resistance to the weakening effects of moisture. The data obtained from mechanical testing demonstrated that the PEDOT had no significant impact on the mechanical properties[46,47,48,49].

In summary, this work described protocols for the preparation of nanofiber materials using commodity polymer substrates that are then coated with EAPs through VPD. The versatility of these methods allows for the preparation of nanofiber materials with tailored fiber diameter and mechanical properties. In addition, these protocols can be adapted for similar materials that utilize nanofibers from commodity polymers other than PAN and coatings with EAPs other than PEDOT, opening the doors to applications in scaffolds for nerve regeneration, water purification, catalysis, and energy storage.

Disclosures

The authors have nothing to disclose.

Acknowledgments

This work was supported in part by the National Science Foundation Partnership for Research and Education in Materials (DMR#2122041) and the Alfred P. Sloan Foundation (# G-2022-19553) Texas State University/ University of Colorado Boulder Sloan Undergraduate Research Program.

References

1. Keirouz, A.et al. The history of electrospinning: Past, present, and future developments. *Adv Mater Technol.* **8** (11), 2201723 (2023).
2. Shi, S.et al. Recent progress in protective membranes fabricated via electrospinning: Advanced materials, biomimetic structures, and functional applications. *Adv Mater.* **34** (17), 31 (2022).
3. Bhardwaj, N., Kundu, S. C. Electrospinning: A fascinating fiber fabrication technique. *Biotechnol Adv.* **28** (3), 325-347 (2010).
4. Huang, Z. M., Zhang, Y. Z., Kotaki, M., Ramakrishna, S. A review on polymer nanofibers by electrospinning and their applications in nanocomposites. *Compos Sci Technol.* **63** (15), 2223-2253 (2003).
5. Sill, T. J., von Recum, H. A. Electrospinning: Applications in drug delivery and tissue engineering. *Biomaterials.* **29** (13), 1989-2006 (2008).
6. Cheng, Y., Zhu, W., Lu, X., Wang, C. Recent progress of electrospun nanofibrous materials for electromagnetic interference shielding. *Compos Commun.* **27,** 100823 (2021).
7. Ramakrishna, S., Fujihara, K., Teo, W. E., Lim, T. C., Ma, Z. *An introduction to electrospinning and nanofibers.* World Scientific Publishing Co (2005).
8. Li, D., Xia, Y. Electrospinning of nanofibers: Reinventing the wheel? *Adv Mater.* **16** (14), 1151-1170 (2004).
9. Greiner, A., Wendorff, J. H. Electrospinning: A fascinating method for the preparation of ultrathin fibers. *Angew Chem Int Ed.* **46** (30), 5670-5703 (2007).
10. Cheng, Y., Zhu, W., Lu, X., Wang, C. Mechanically robust, stretchable, autonomously adhesive, and environmentally tolerant triboelectric electronic skin for self-powered healthcare monitoring and tactile sensing. *Nano Energy.* **102,** 107636 (2022).
11. Zhu, W., Cheng, Y., Wang, C., Lu, X. Fabrication of a tubular cuo/nio biomimetic nanozyme with synergistically promoted peroxidase-like performance for isoniazid sensing. *Inorg Chem.* **61** (41), 16239-16247 (2022).
12. Zhu, W., Cheng, Y., Wang, C., Pinna, N., Lu, X. Transition metal sulfides meet electrospinning: Versatile synthesis, distinct properties and prospective applications. *Nanoscale.* **13** (20), 9112-9146 (2021).
13. Rasmussen, S. C. Conjugated and conducting organic polymers: The first 150 years. *ChemPlusChem.* **85** (7), 1412-1429 (2020).
14. Balint, R., Cassidy, N. J., Cartmell, S. H. Conductive polymers: Towards a smart biomaterial for tissue engineering. *Acta Biomater.* **10** (6), 2341-2353 (2014).
15. Luo, C. J., Nangrejo, M., Edirisinghe, M. A novel method of selecting solvents for polymer electrospinning. *Polymer.* **51** (7), 1654-1662 (2010).
16. Avossa, J., Herwig, G., Toncelli, C., Itel, F., Rossi, R. M. Electrospinning based on benign solvents: Current definitions, implications and strategies. *Green Chem.* **24** (6), 2347-2375 (2022).

17. Ding, Y., Hou, H., Zhao, Y., Zhu, Z., Fong, H. Electrospun polyimide nanofibers and their applications. *Prog Polym Sci.* **61,** 67-103 (2016).
18. Ahmadi Bonakdar, M., Rodrigue, D. Electrospinning: Processes, structures, and materials. *Macromol.* **4** (1), 58-103 (2024).
19. Donglin, X., Man, X., Jianzhuang, L., Xiujian, Z. Co-electrodeposition and characterization of cu (in, ga)se2 thin films. *J Mater Sci.* **41** (7), 1875-1878 (2006).
20. Rahman, M. H.*et al. Recent progress on electroactive polymers: Synthesis, properties and applications. Ceramics.* **4** (3), 516-541 (2021).
21. Manawi, Y. M., Ihsanullah, S. A., Al-Ansari, T., Atieh, M. A. A review of carbon nanomaterials' synthesis via the chemical vapor deposition (cvd) method. *Materials.* **11** (5), 822 (2018).
22. Zhu, W., Cheng, Y., Wang, C., Lu, X. Rational construction of particle-in-tube structured nio/coo/ polypyrrole as efficient nanozyme for biosensing. *Sens Actuators B Chem.* **370,** 132442 (2022).
23. Sapountzi, E., Chateaux, J. F., Lagarde, F. Combining electrospinning and vapor-phase polymerization for the production of polyacrylonitrile/ polypyrrole core-shell nanofibers and glucose biosensor application. *Front Chem.* **8**, 1-10 (2020).
24. Acosta, M., Santiago, M. D., Irvin, J. A. Electrospun conducting polymers: Approaches and applications. *Materials.* **15** (24), 8820 (2022).
25. Wei, W.et al. Advancing nanofiber research: Assessing nonsolvent contributions to structure using coaxial electrospinning. *Langmuir.* **39** (31), 10881-10891 (2023).
26. Islam, M.*et al. Electrospun carbon nanofibre-assisted patterning of metal oxide nanostructures. Microsyst Nanoeng.* **8** (1), 71 (2022).
27. Xue, J., Wu, T., Dai, Y., Xia, Y. Electrospinning and electrospun nanofibers: Methods, materials, and applications. *Chem Rev.* **119** (8), 5298-5415 (2019).
28. Wissmann, P. J., Grover, M. A. Optimization of a chemical vapor deposition process using sequential experimental design. *Ind End Chem Res.* **49** (12), 5694-5701 (2010).
29. Ghafourisaleh, S., Popov, G., Leskelä, M., Putkonen, M., Ritala, M. Oxidative mld of conductive pedot thin films with edot and recl5 as precursors. *ACS Omega.* **6** (27), 17545-17554 (2021).
30. Teo, W. E., Ramakrishna, S. A review on electrospinning design and nanofibre assemblies. *Nanotechnology.* **17** (14), R89 (2006).
31. Cao, Q.et al. Effect of sonication treatment on electrospinnability of high-viscosity pan solution and mechanical performance of microfiber mat. *Iran Polym J.* **23** (12), 947-953 (2014).
32. Garrudo, F. F. F.*et al. Production of blended poly(acrylonitrile): Poly(ethylenedioxythiophene):Poly(styrene sulfonate) electrospun fibers for neural applications. Polymers.* **15** (13), 2760 (2023).
33. Kayser, L. V., Lipomi, D. J. Stretchable conductive polymers and composites based on pedot and pedot:Pss. *Adv Mater.* **31** (10), 1806133 (2019).
34. Abu Owida, H., Al-haj Moh'd, B. A,l Takrouri, M. Designing an integrated low-cost electrospinning device

for nanofibrous scaffold fabrication. *HardwareX.* **11,** e00250 (2022).

35. Agarwal, S., Greiner, A., Wendorff, J. H. Functional materials by electrospinning of polymers. *Prog Polym Sci.* **38** (6), 963-991 (2013).
36. Vasita, R., Katti, D. S. Nanofibers and their applications in tissue engineering. *Int J Nanomedicine.* **1** (1), 15-30 (2006).
37. Huang, Z.-M., Zhang, Y.-Z., Kotaki, M., Ramakrishna, S. A review on polymer nanofibers by electrospinning and their applications in nanocomposites. *Compos Sci Technol.* **63** (15), 2223-2253 (2003).
38. Koski, A., Yim, K., Shivkumar, S. Effect of molecular weight on fibrous pva produced by electrospinning. *Matter Lett.* **58** (3-4), 493-497 (2004).
39. Fong, H., Chun, I., Reneker, D. H. Beaded nanofibers formed during electrospinning. *Polymer.* **40** (16), 4585-4592 (1999).
40. Liu, Y., He, J. H., Yu, J. Y., Zeng, H. M. Controlling numbers and sizes of beads in electrospun nanofibers. *Polym Int.* **57** (4), 632-636 (2008).
41. Beachley, V., Wen, X. Effect of electrospinning parameters on the nanofiber diameter and length. *Matter Sci Eng C.* **29** (3), 663-668 (2009).
42. Matthews, J. A., Wnek, G. E., Simpson, D. G., Bowlin, G. L. Electrospinning of collagen nanofibers. *Biomacromolecules.* **3** (2), 232-238 (2002).
43. Asatekin, A.*et al. Designing polymer surfaces via vapor deposition. Mater Today.* **13** (5), 26-33 (2010).
44. Butler, J. H., Joy, D. C., Bradley, G. F., Krause, S. J. Low-voltage scanning electron microscopy of polymers. *Polymer.* **36** (9), 1781-1790 (1995).
45. Wu, J., Xiao, M., Quezada-Renteria, J. A., Hou, Z., Hoek, E. M. V. Sample preparation matters: Scanning electron microscopic characterization of polymeric membranes. *JMS Letters.* **4** (1), 100073 (2024).
46. El-Aufy, A. K. *Nanofibers and nanocomposites poly(3,4-ethylene dioxythiophene)/poly(styrene sulfonate) by electrospinning.* Drexel Universit (2004).
47. Pires, L. S., Melo, D. S., Borges, J. P., Henriques, C. R. Pedot-coated pla fibers electrospun from solutions incorporating fe(iii)tosylate in different solvents by vapor-phase polymerization for neural regeneration. *Polymers.* **15** (19), 4004 (2023).
48. Budday, S., Ovaert, T. C., Holzapfel, G. A., Steinmann, P., Kuhl, E. Fifty shades of brain: A review on the mechanical testing and modeling of brain tissue. *Arch Comput Methods Eng.* **27** (4), 1187-1230 (2020).
49. Pham, T. A.*et al.* Investigation on the microscopic/macroscopic mechanical properties of a thermally annealed nafion membrane. *Polymers.* **13** (22), 4018 (2021).